Electronic Supplementary Material (ESI) for Journal of Materials Chemistry C.

Supporting information for

Polymorphism manipulating topo-photochemical reaction, photoactuation, mechanofluorochromism of benzimidazoleylaryl acrylonitriles

Cheng Liu, Jingbo Sun,* Chao Chen, Kaiqi Ye,* Haoran Wang, Xiqiao Yang, Yuan Yue, Ran Lu*

State Key Laboratory of Supramolecular Structure and Materials, College of Chemistry, Jilin University, Changchun, China

E-mail: sunjb@jlu.edu.cn; yekq@jlu.edu.cn; luran@mail.jlu.edu.cn

Video S1. The photo-induced cracking and photosalient behaviors of the sheet-like crystal of *E*-**CN-BIFPh** upon irradiated by 365 nm light.

Video S2. The photo-induced bending of the needle-like crystal of *Z*-**BIFPh-CN** upon irradiated by 365 nm light.

Video S3. The photo-induced bending of the needle-like crystal of *E*-**CN-BINa** upon irradiated by 365 nm light.

General Information

^{1}H NMR and ^{13}C NMR spectra were recorded with Bruker-Avance III 400 MHz and 101 MHz spectrometers using $CDCl_3$ and DMSO-d_6 as solvents and tetramethylsilane (TMS) as the internal standard. The samples for irradiation time-dependent ^{1}H NMR measurements were gained via the irradiation of the microcrystals of *Z*-**BIFPh-CN**, *E*-**CN-BIFPh**, and *E*-**CN-BINa** by 365 nm (16.7 mW/cm^2) light for different times, followed by dissolving in DMSO-d_6. FT-IR spectra were obtained with a Nicolet-360 FT-IR spectrometer by incorporating samples into KBr disks. High-resolution mass spectra were performed on an Agilent 1290 Infinity LC system coupled with Bruker micro TOF QII mass spectrometer. UV-vis absorption spectra were measured by a Shimadzu UV-1601PC spectrophotometer. Fluorescence emission spectra were taken on a Shimadzu RF5301 luminescence spectrometer. The solid-state samples for the absorption and emission measurements were prepared by smearing the powders on the quartz plate with a spatula. Differential scanning calorimetry (DSC) was performed on Perkin-Elmer Diamond DSC with a heating rate of 10 °C/min under a nitrogen atmosphere. Powder X-ray diffraction patterns were obtained on Empyrean XRD equipped with graphite monochromatized Cu-Kα radiation (λ = 1.5418 Å) employing a scanning rate of 0.00267°/s in the 2θ range of 5-40° and the samples were kept at room temperature during data collection. Single crystals of *E*-**CN-BIFPh** in G-phase and OR-phase, D-**CN-BIFPh**, *Z*-**BIFPh-CN** in G-phase, and *E*-**CN-BINa** were selected for single crystal X-ray diffraction analysis on a Rigaku RAXIS-RA PID diffractometer using graphite-monochromated Mo-Kα radiation (λ = 0.71073 Å), and the crystals were kept at -173 ºC during data collection, except for *E*-**CN-BIFPh** in OR-phase which was measured at room temperature. The structures were solved by the direct methods and refined on F2 by full-matrix least-square using the SHELXTL-97 program. The fluorescence quantum yields and the fluorescence lifetimes were measured on Edinburgh Instrument FLS920. An integrating sphere was used for the measurement of the solid-state fluorescence quantum yield. All the reagents were used without further purification.

Preparation of the crystals: The crystals of *E*-**CN-BIFPh** in G-phase and in OR-phase were prepared by evaporation from the solutions in dichloromethane/ethyl acetate (v/v = 1/3) in a fast/slow evaporation rate. The crystals of *Z*-**BIFPh-CN** in G-phase and *E*-**CN-BINa** were prepared by slow evaporation from the solutions in dichloromethane/petroleum ether (v/v = 1/3). The crystals of *Z*-**BIFPh-CN** in B-phase were prepared by fast evaporation of dichloromethane/petroleum ether (v/v = 1/3). The prepared crystals were used in single-crystal X-ray diffraction measurement and the study of stimuli-responsive properties.

Investigations of the photomechanical effects: The crystals were first placed on the glass substrates or stuck at the needle tip/the end of the glass substrates. Then, the hand-held flashlight (365 nm, 16.7 mW/cm^2) was used as the light source to irradiate the crystals at a distance of ca. 2 cm. The photomechanical motions were observed using optical microscopy or by naked eyes, and recorded by Mi 10S.

Theoretical calculations: HOMO and LUMO plots as well as electrostatic potential (ESP) were calculated by using Gaussian 16W and analyzed by GaussView 6.0.[1-2] The nature transition orbits (NTOs) were calculated by using Gaussian 16W and analyzed by Multiwfn.[3]

Synthesis

(*Z*)-3-(1*H*-benzo[d]imidazol-2-yl)-2-(4-fluorophenyl)acrylonitrile (*Z*-**BIFPh-CN**)

Sodium hydroxide (0.07 g, 1.64 mmol) was dissolved in ethanol (30 mL) in a 100 mL round bottom flask, and then, 1*H*-benzo[d]imidazole-2-carbaldehyde (0.2 g, 1.37 mmol) was added. After that, 2-(4-fluorophenyl)acetonitrile (0.22 g, 1.64 mmol) in ethanol (10 mL) was added dropwise. After stirring for 5 h, the reaction mixture was poured into water (200 mL). The yellow precipitation was collected via filtration over a Buchner funnel. The filter cake was added to dichloromethane, and the precipitation was removed. Subsequently, the saturated dichloromethane solution was poured into petroleum ether (4 times of V_{DCM}) to afford the yellow solid (0.22 g, yield 45%). Mp: 145.0-147.0 °C. ^{1}H NMR (400 MHz, DMSO-d_6) δ ppm 12.76 (s, 1H), 7.86 (t, J = 6.4 Hz, 2H), 7.79 (s, 1H), 7.70-7.68 (m, 2H), 7.42 (t, J = 8.0 Hz, 2H), 7.31-7.29 (m, 2H), (Figure S27). ^{13}C NMR (101 MHz, $CDCl_3$) δ ppm163.91 (d, J = 253.6 Hz), 145.90, 130.55 (d, J = 1.9 Hz), 128.29 (d, J = 3.5 Hz), 128.02 (d, J = 8.7 Hz), 124.91, 118.50, 116.85, 116.63, 112.43 (Figure S28). FT-IR (KBr, cm^{-1}): 3400.80, 3360.64, 3064.00, 2220.90, 1605.11, 1596.93, 1514.41, 1416.58, 1309.62, 1279.64, 1234.85, 1221.49, 1173.37, 1164.87, 854.95, 833.77, 739.28, 706.74, 604.98, 577.61, 511.28. HPLC-MS: Calcd. For $C_{16}H_{10}FN_3$ 264.0939, found: 264.0932 $[M+H]^+$ (Figure S29).

(*E*)-2-(1*H*-benzo[d]imidazol-2-yl)-3-(4-fluorophenyl)acrylonitrile (*E*-**CN**-**BIFPh**)

The synthetic method for *E*-**CN**-**BIFPh** was similar to that of *Z*-**BIFPh-CN**. It was synthesized from 2-(1*H*-benzo[d]imidazol-2-yl)acetonitrile (0.3 g, 1.9 mmol) and 4-fluorobenzaldehyde (0.2 g, 1.6 mmol). The crude product was purified by reprecipitation of the saturated dichloromethane solution in petroleum ether (V_{DCM}/V_{PE}=1/4). Yellow solid of *E*-**CN**-**BIFPh** (0.31 g) was obtained in a yield of 54 %. Mp: 187.0-189.0 °C. ^{1}H NMR (400 MHz, DMSO-d_6) δ ppm 13.09 (s, 1H), 8.36 (s, 1H), 8.07 (dd, J = 8.4 Hz, J = 5.6 Hz, 2H), 7.64 (d, J = 32.4 Hz, 2H), 7.48 (t, J = 8.8 Hz, 2H), 7.27 (s, 2H), (Figure S30). ^{13}C NMR (101 MHz, $CDCl_3$) δ ppm 164.70 (d, J = 256.9 Hz), 146.10, 145.46, 132.39 (d, J = 9.0 Hz), 128.94 (d, J = 3.2 Hz), 123.99, 116.77, 116.68, 116.55, 99.40 (Figure S31). FT-IR (KBr, cm^{-1}): 3305.04, 3063.01, 2233.51, 1596.40, 1506.34, 1436.43, 1416.29, 1317.84, 1275.98, 12452.35, 1162.95, 1118.09, 950.98, 913.06, 824.57, 767.01, 741.87, 631.48, 511.72. HPLC-MS: Calcd. For $C_{16}H_{10}FN_3$ 264.0939, found: 264.0910 $[M+H]^+$ (Figure S32).

(*E*)-2-(1*H*-benzo[d]imidazol-2-yl)-3-(naphthalen-1-yl)acrylonitrile (*E*-**CN**-**BINa**)

The synthetic method for *E*-**CN**-**BINa** was similar to that of *Z*-**BIFPh-CN**. It was synthesized from 2-(1*H*-benzo[d]imidazol-2-yl)acetonitrile (0.24 g, 1.5 mmol) and naphthalene-1-carbaldehyde (0.2 g, 1.28 mmol). The crude product was purified by reprecipitation of the saturated dichloromethane solution in petroleum ether (V_{DCM}/V_{PE}=1/4). Yellow solid of *E*-**CN**-**BINa** (0.26 g) was obtained in a yield of 52 %. Mp: 190.0-192.0 °C. ^{1}H NMR (400 MHz, DMSO-d_6) δ ppm 12.36 (s, 1H), 8.67 (s, 1H), 8.23 (d, J = 7.6 Hz, 1H), 8.04-8.01 (m, 2H), 7.68-7.62 (m, 3H), 7.39-7.29 (m, 3H), 7.22-7.18 (m, 2H) (Figure S33). ^{13}C NMR (101 MHz, $CDCl_3$) δ ppm 147.86, 143.92, 133.62, 132.08, 131.51, 130.36, 129.37, 127.96, 127.57, 127.35, 126.06, 124.22, 123.69, 123.68, 123.67, 116.47, 106.55 (Figure S34). FT-IR (KBr, cm^{-1}): 3072.82, 2890.57, 2765.89, 2226.67, 1621.08, 1599.70, 1571.64, 1508.50, 1440.16, 1421.29, 1333.17, 1312.89, 1278.07, 1242.20, 973.61, 900.63, 799.38, 777.21, 767.20, 749.33, 636.77, 437.52. HPLC-MS: Calcd. For $C_{20}H_{13}N_3$ 296.1189, found: 296.1159 $[M+H]^+$ (Figure S35).

Table S1 The calculated molecular conformation, dihedral angles between benzoimidazole and benzene/naphthalene rings, and dipole moments for *E*-**CN-BINa**, *D*-**CN-BIFPh**, and *Z*-**CN-BIFPh** at ground states in vacuo.

	Z-**BIFPh-CN**	*E*-**CN-BIFPh**	*E*-**CN-BINa**
Molecular conformation	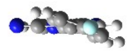	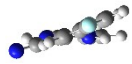	
Dihedral angle	21.1	20.5	48.8
Dipole moment (Debye)	0.40	6.33	6.82

Table S2 The calculated molecular conformation, dihedral angles between benzoimidazole and benzene/naphthalene rings, and dipole moments for *E*-**CN-BINa**, D-**CN-BIFPh** and *Z*-**CN-BIFPh** at excited states.

	Z-**BIFPh-CN***	*E*-**CN-BIFPh***	*E*-**CN-BINa***
Molecular conformation		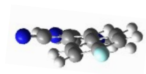	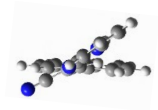
Dihedral angle	10.9	28.9	36.0
Dipole moment (Debye)	1.05	10.10	9.30

Table S3 Single crystal data and structure refinement for *Z*-**BIFPh-CN** in G-phase, *E*-**CN**-**BIFPh** in G-phase, *E*-**CN**-**BINa** in OR-phase, *E*-**CN**-**BINa** and D-**CN**-**BIFPh**.

	Z-**BIFPh-CN** in G-phase	*E*-**CN-BIFPh** in G-phase	*E*-**CN-BIFPh** in OR-phase	*E*-**CN-BINa**	D-**CN-BIFPh**
Formula	$C_{16}H_{10}FN_3$	$C_{16}H_{10}FN_3$	$C_{16}H_{10}FN_3$	$C_{20}H_{13}N_3$	$C_{32}H_{20}F_2N_6$
Formula weight	263.27	263.27	263.27	295.33	526.54
Space group	$P2_1/n$	$C2$/c	$P2_1/n$	$P2_1/n$	$C2$/c
Crystal system	monoclinic	monoclinic	monoclinic	monoclinic	monoclinic
a/Å	15.8850(6)	12.8656(5)	6.7580(3)	9.5049(7)	23.6834(9)
b/Å	7.1306(2)	6.7384(3)	28.3322(12)	18.4000(12)	12.4341(5)
c/Å	22.5916(8)	28.4952(12)	7.3254(3)	17.9978(13)	21.9726(7)
α/deg	90	90	90	90	90
β/deg	103.786(2)	99.610(2)	116.4820(10)	93.843(2)	98.0540(10)
γ/deg	90	90	90	90	90
Volume/ $Å^3$	2485.22(15)	2435.68(18)	1255.42(9)	3140.6(4)	6406.7(4)
Z	4	8	4	8	8
D(calc)/g cm^{-3}	1.407	1.436	1.393	1.249	1.092
μ/mm^{-1}	0.097	0.099	0.096	0.076	0.075
Final R indexes [I>2sigma(I)]	$R_1 = 0.0483$ $wR_2 = 0.0967$	$R_1 = 0.0471$ $wR_2 = 0.1234$	$R_1 = 0.0604$ $wR_2 = 0.1440$	$R_1 = 0.0835$ $wR_2 = 0.1657$	$R_1 = 0.0523$ $wR_2 = 0.1246$
R indexes (all data)	$R_1 = 0.0882$ $wR_2 = 0.1169$	$R_1 = 0.0659$ $wR_2 = 0.1389$	$R_1 = 0.0943$ $wR_2 = 0.1670$	$R_1 = 0.1287$ $wR_2 = 0.1850$	$R_1 = 0.1020$ $wR_2 = 0.1574$
GoF	1.011	1.036	1.049	1.082	1.005
CCDC	2240227	2240229	2240230	2240231	2240226

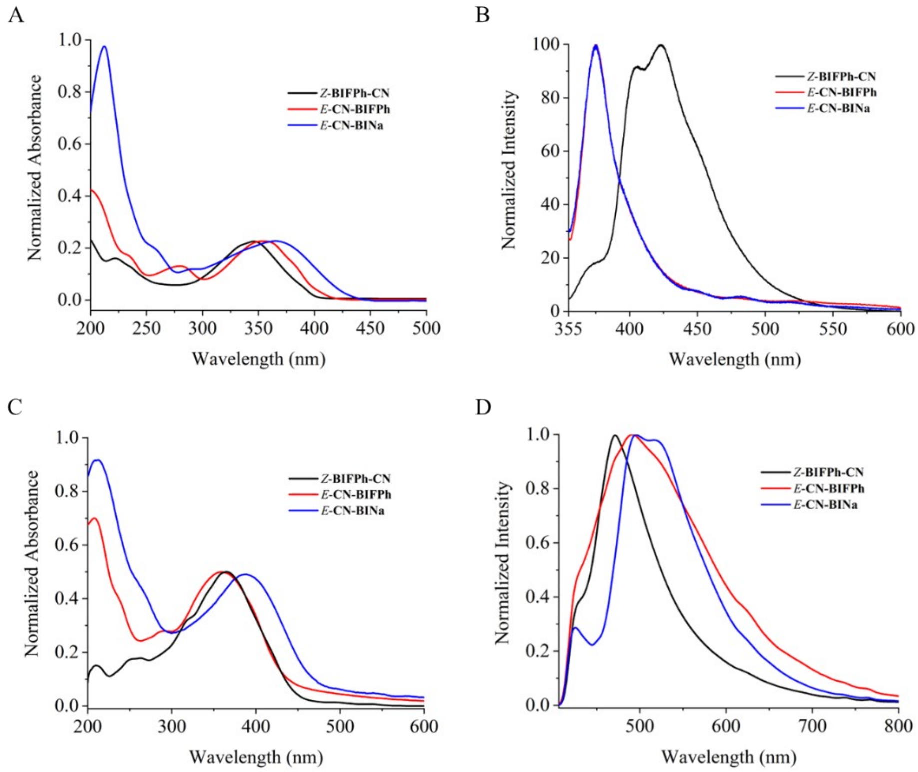

Figure S1 Normalized UV-vis absorption and fluorescence emission spectra of *Z*-**BIFPh-CN**, *E*-**CN-BIFPh**, and *E*-**CN-BINa** in cyclohexane (A and B, 1.0×10^{-5} M, λ_{ex} = 337 nm) and powders (C and D, λ_{ex} = 365 nm).

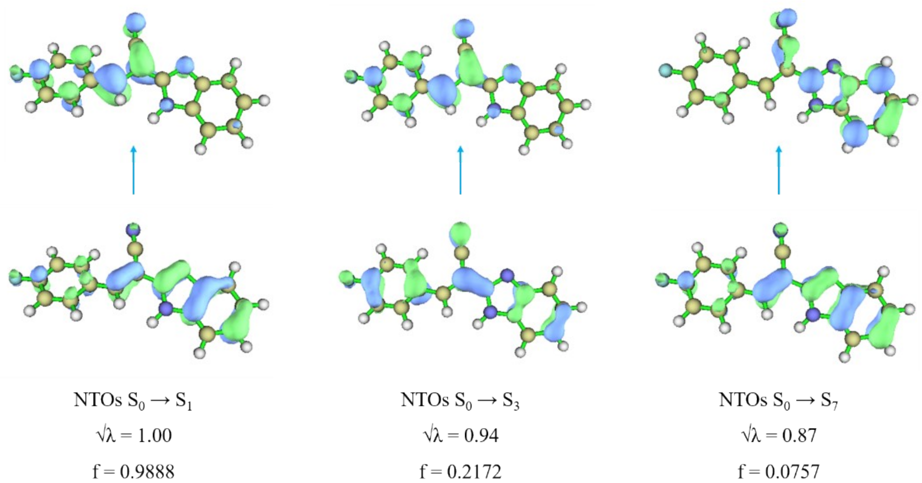

Figure S2 NTOs (natural transition orbitals) of *E*-**CN-BIFPh** in cyclohexane calculated by the Gaussian 16W with TD/6-31G(d,p)/RB3LYP basis set. Parameter λ and f refer to the associated eigenvalues of NTOs and oscillator strength, respectively.

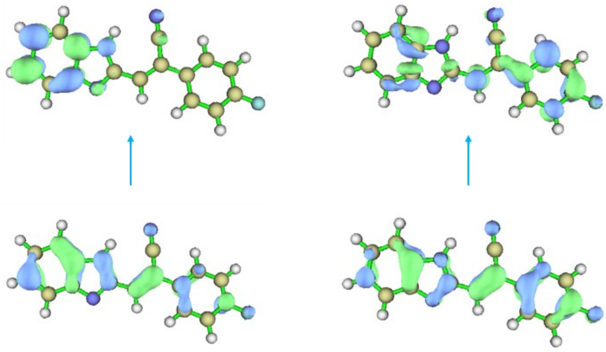

Figure S3 NTOs of *Z*-**BIFPh-CN** in cyclohexane calculated by the Gaussian 16W with TD/6-31G(d,p)/RB3LYP basis set. Parameter λ and f refer to the associated eigenvalues of NTOs and oscillator strength, respectively.

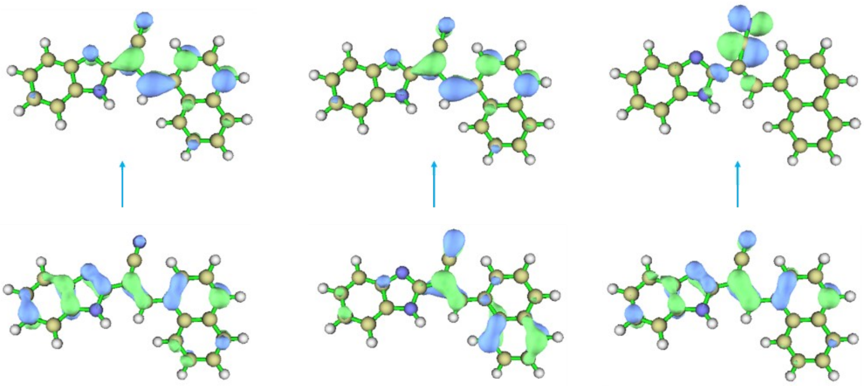

Figure S4 NTOs of *E*-**CN-BINa** in cyclohexane calculated by the Gaussian 16W with TD/6-31G(d,p)/RB3LYP basis set. Parameter λ and f refer to the associated eigenvalues of NTOs and oscillator strength, respectively.

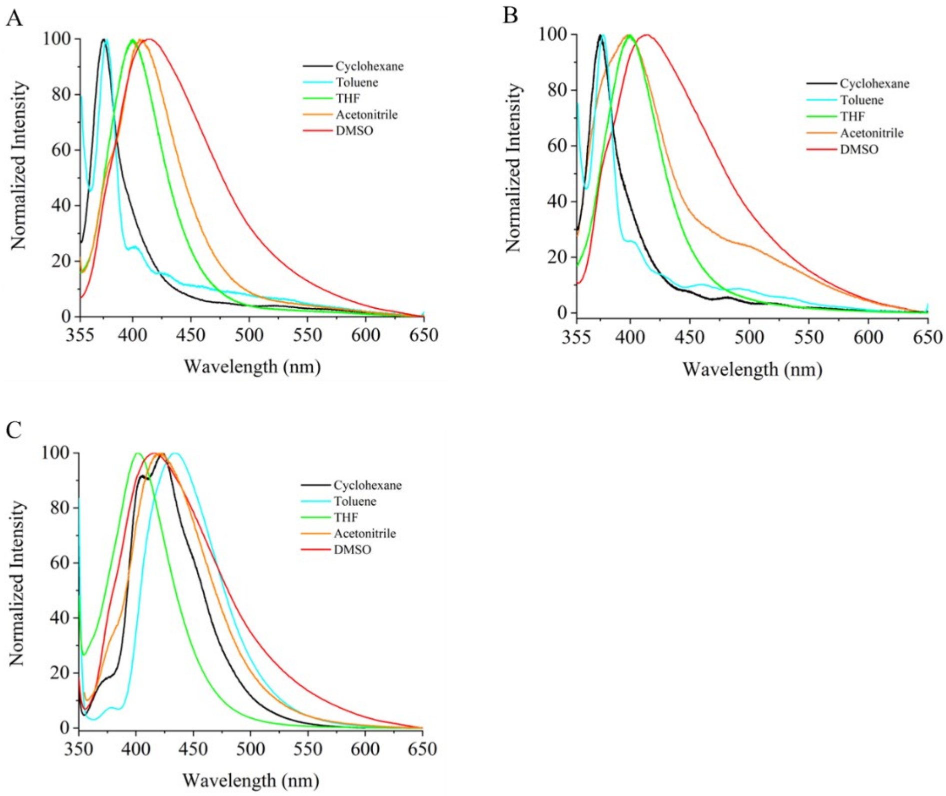

Figure S5 Normalized fluorescence emission spectra of *E*-**CN**-**BIFPh** (A), *E*-**CN**-**BINa** (B) and *Z*-**BIFPh-CN** (C) in different solvents (1.0×10^{-5} M, λ_{ex} = 337 nm).

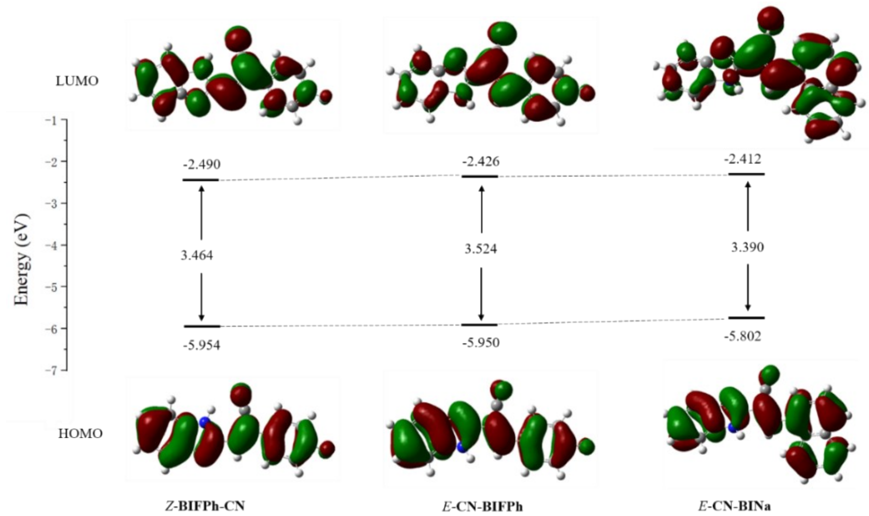

Figure S6 The frontier molecular orbital plots and energy levels for the HOMOs and LUMOs of *Z*-**BIFPh-CN**, *E*-**CN**-**BIFPh**, and *E*-**CN**-**BINa** in vacuo.

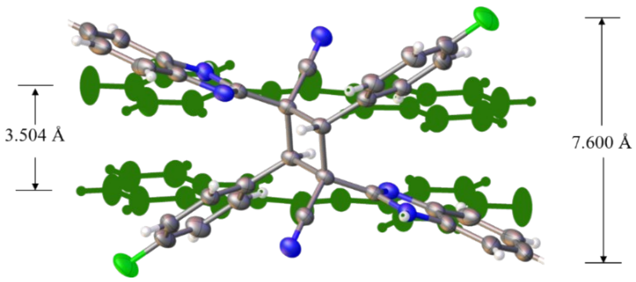

Figure S7 The lengths as well as the widths for the π-dimer of *E*-**CN-BIFPh** (green) and D-**CN-BIFPh** (gray) in single crystals.

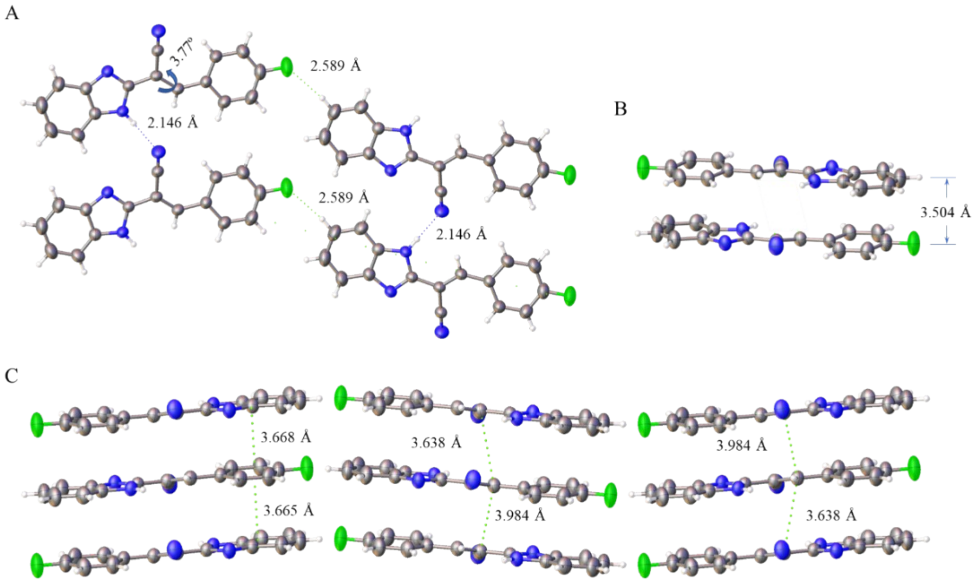

Figure S8 (A) Molecular packing in the single crystal of *E*-**CN-BIFPh** in OR-phase viewed along the c-axis, the distances corresponding to C–H···F (green) and C–H···N (blue) hydrogen bonds and the dihedral angles between the phenyl and the benzimidazole rings; (B) The distance between two molecules in a π-dimer; (C) Molecular packing viewed along the a-axis and the center-to-center distance between the adjacent double bonds.

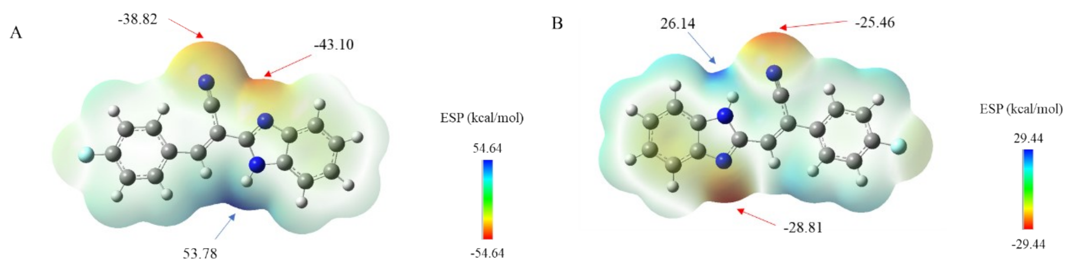

Figure S9 Calculated electron density mapped with the electrostatic potential of *E*-**CN-BIFPh** (a) and *Z*-**BIFPh-CN** (b), based on their optimized structures, determined using DFT at the B3LYP/6-31G(d) level. The units are in kcal/mol.

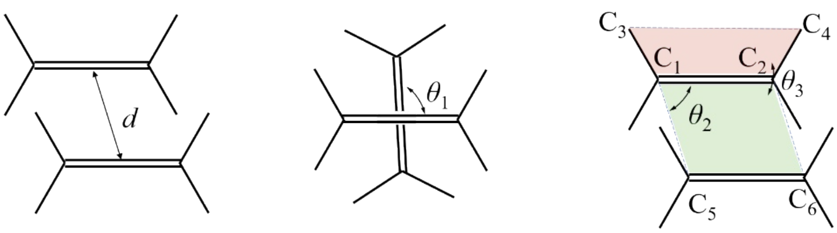

Scheme S1 Geometrical parameters used in the relative representation of reactant double bonds. *d* is the distance between the centers of the two potential reactive carbon-carbon double bonds; θ_1 refers to the rotational angle between two double bonds; θ_2 is the angle of the parallelogram formed by C_1, C_2, C_5, and C_6; θ_3 corresponds to the dihedral angle between green and pink plane.-

Table S4 Relative orientations of the adjacent parallel double bonds of *Z*-**BIFPh-CN** in G-phase, *E*-**CN-BIFPh** in G-phase, and *E*-**CN-BIFPh** in OR-phase.*

	d (Å)	θ_1 (°)	θ_2 (°)	θ_3 (°)
Z-**BIFPh-CN** in G-phase	4.541	10.06	122.16	114.50
E-**CN-BIFPh** in G-phase	4.432	89.70	117.98	
E-**CN-BIFPh** in OR-phase	3.638	0	110.83	92.37
ideal values	< 4.20	0	90	90

*For a definition of geometrical parameters see Scheme S1.

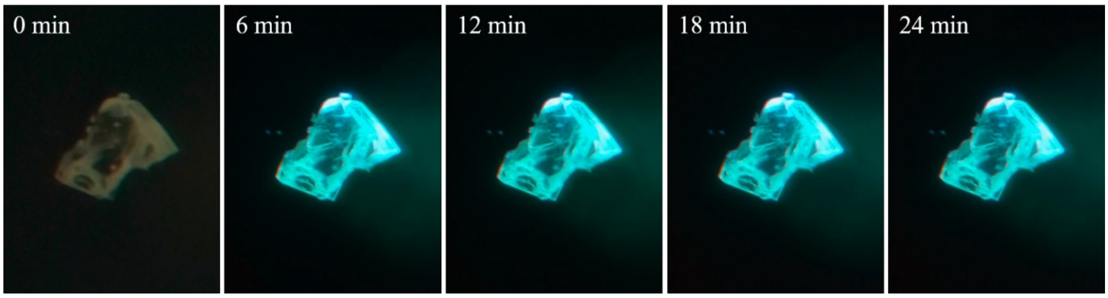

Figure S10 Optical microscope photos of the block-like crystal of *E*-**CN-BIFPh** in G-phase upon irradiation by 365 nm light (16.7 mW/cm^2) for different times.

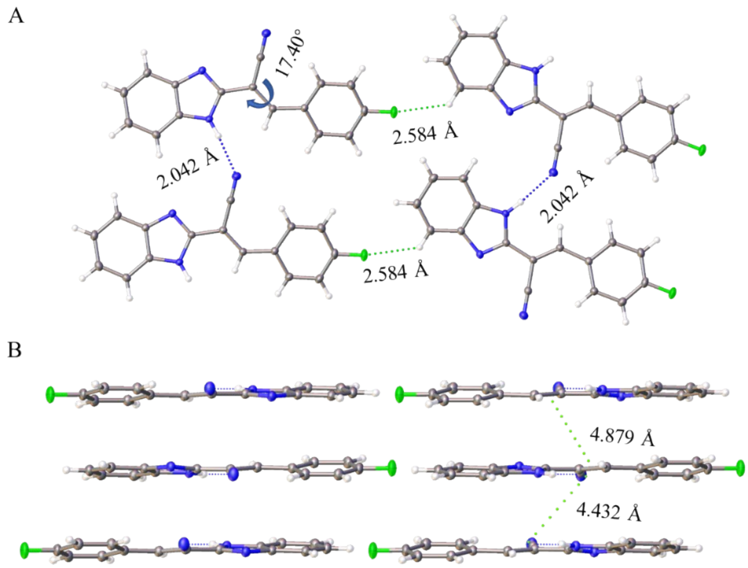

Figure S11 (A) Molecular packing in the single crystal of *E*-**CN-BIFPh** in G-phase viewed along the a-axis, the distance of C–H···F (green) and C–H···N (blue) hydrogen bonds and the dihedral angles between phenyl and benzimidazole ring; (B) Molecular packing viewed along the b-axis and the center-to-center distance between the adjacent double bonds.

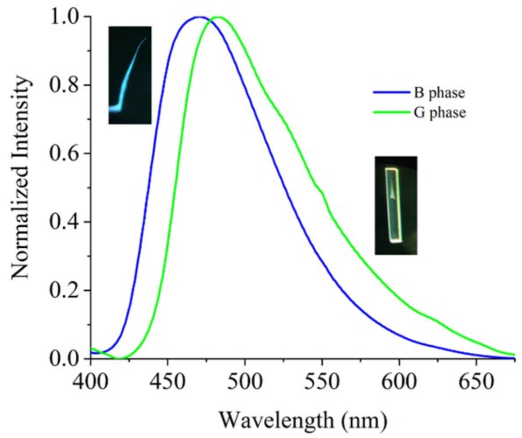

Figure S12 Normalized fluorescence emission spectra (λ_{ex} = 365 nm) of *Z*-**BIFPh-CN** in B-phase and in G-phase crystals. Insets: the photos of the crystals under UV light.

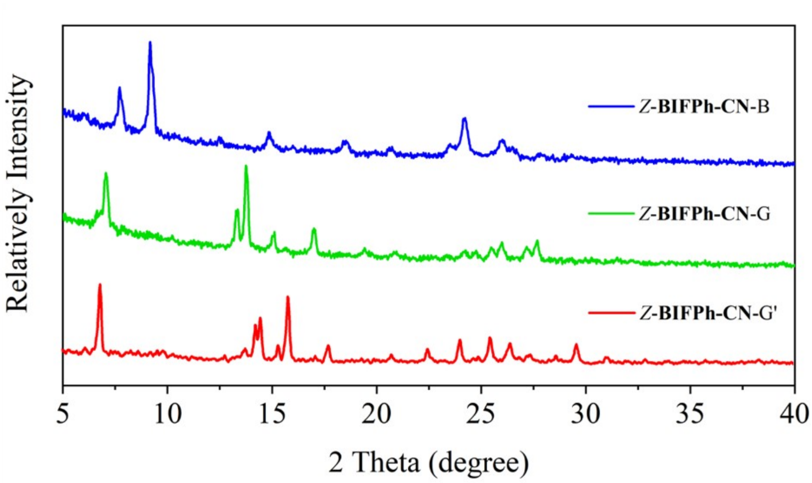

Figure S13 PXRD patterns of B-phase crystals of *Z*-**BIFPh-CN** (blue), G-phase crystals of *Z*-**BIFPh-CN** before (green) and after (red) heating.

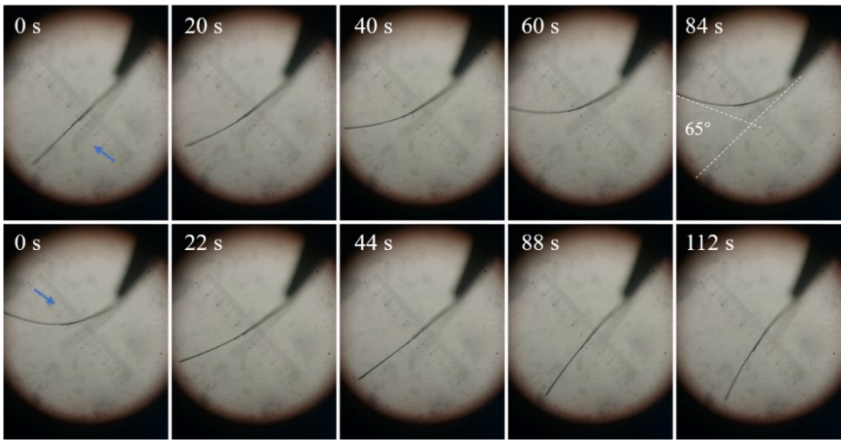

Figure S14 Optical microscope photos of the needle-like crystal of *Z*-**BIFPh-CN** upon irradiation by 365 nm light (16.7 mW/cm^2) for different times (the blue arrows indicate the irradiation directions).

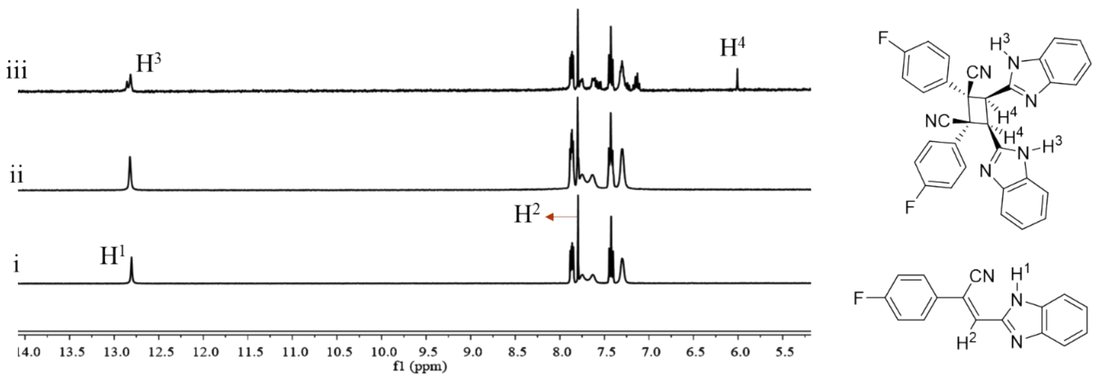

Figure S15 ^{1}H NMR spectra of *Z*-**BIFPh-CN** before (i) and after irradiating the G-phase crystals (ii) and B-phase crystals (iii) with 365 nm light (16.7 mW cm^{-2}) for 1 h followed by dissolution in DMSO-d_6.-

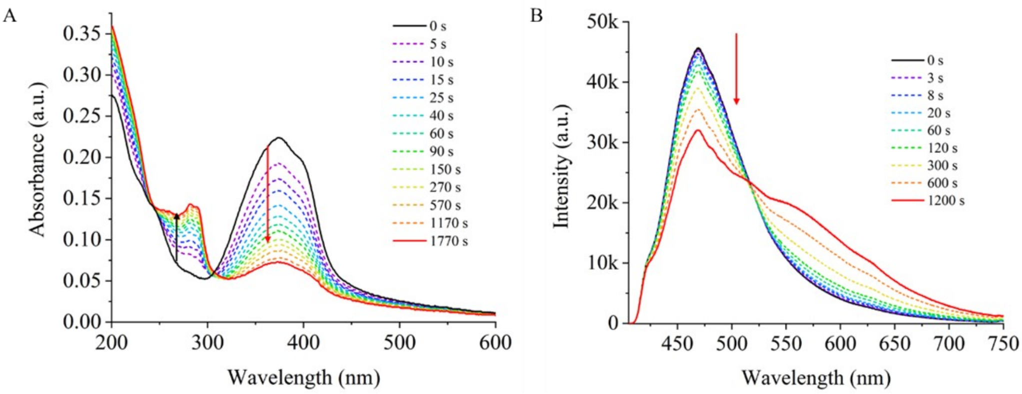

Figure S16 UV-vis absorption (A) and fluorescence emission (B, λ_{ex} = 375 nm) spectra of *Z*-**BIFPh-CN** in B-phase crystals before and after irradiation by 365 nm light (16.7 mW cm^{-2}) for different times.

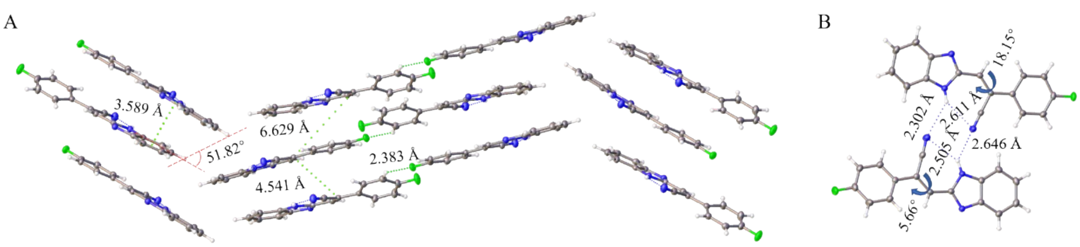

Figure S17 (A) Molecular packing in the single crystal of *Z*-**BIFPh-CN** in G-phase viewed along the c-axis, the distance between the adjacent double bonds and the distance of C–H···F hydrogen bond; (B) The distance of C–H···N hydrogen bonds and the dihedral angles between phenyl and benzimidazole rings.

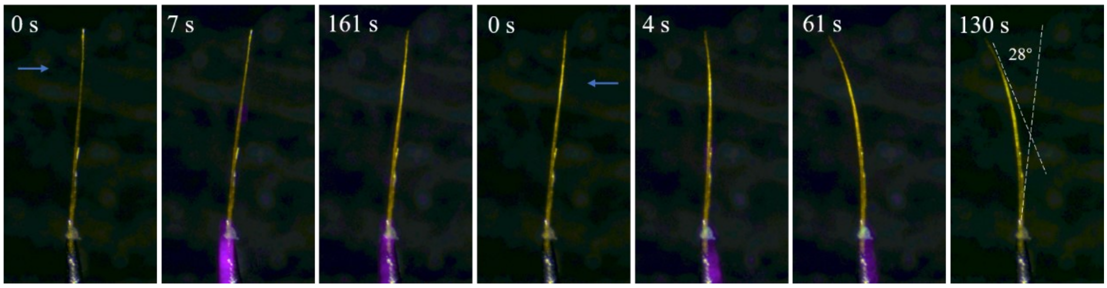

Figure S18 Optical microscope photos of the needle-like crystal of *E*-**CN**-**BINa** upon irradiation by 365 nm light (16.7 mW/cm^2) at different times (the blue arrows indicate the irradiation directions).

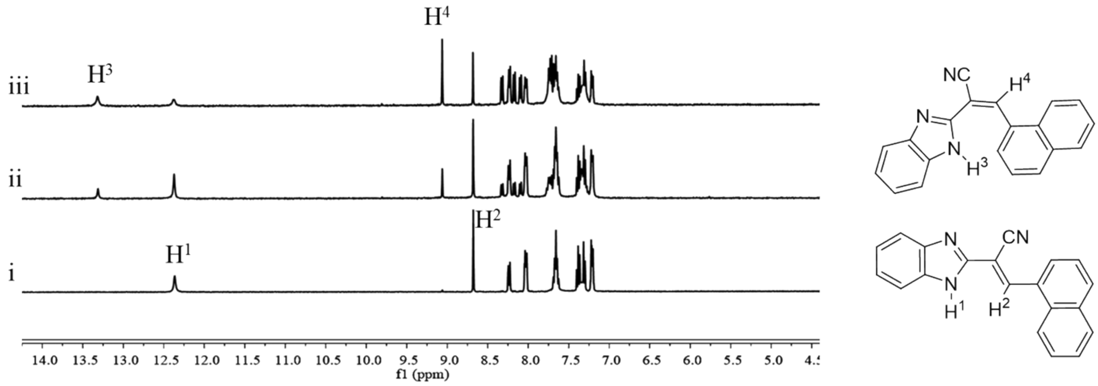

Figure S19 ^{1}H NMR spectra of *E*-**CN-BINa** before (black) and after (blue) irradiation with 365 nm light (16.7 mW cm^{-2}) for 5 min in DMSO-d_6 and ^{1}H NMR spectrum of *E*-**CN-BINa** after irradiating microcrystals (red) with 365 nm light (16.7 mW cm^{-2}) for 1 h followed by dissolution in DMSO-d_6.

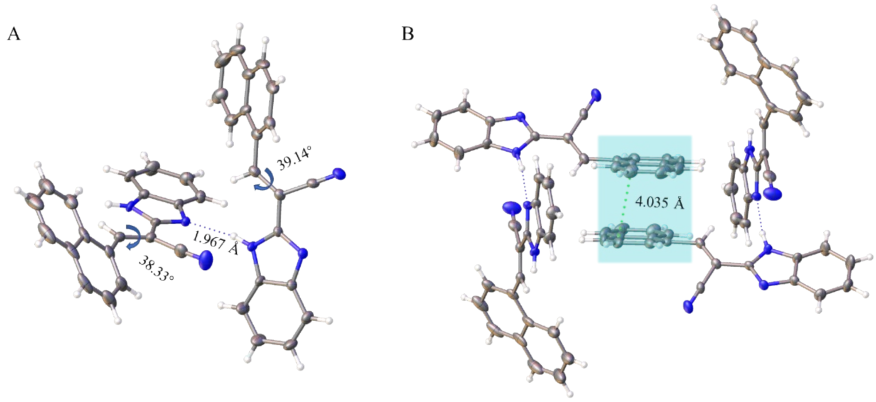

Figure S20 The single crystal structure of *E*-**CN-BINa** in one asymmetric unit (A) and in two adjacent asymmetric units (B).-

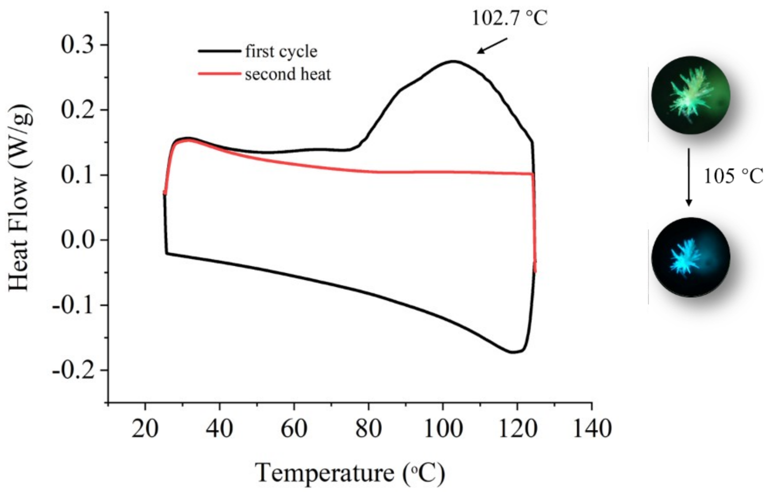

Figure S21 DSC curves of the G-phase crystals of *Z*-**BIFPh-CN** measured at a heating and cooling rate of 10 °C/min under a nitrogen atmosphere. Insets: The photos of the G-phase crystals of *Z*-**BIFPh-CN** under UV light before (upper) and after (lower) heated at 105 °C for 2 min.

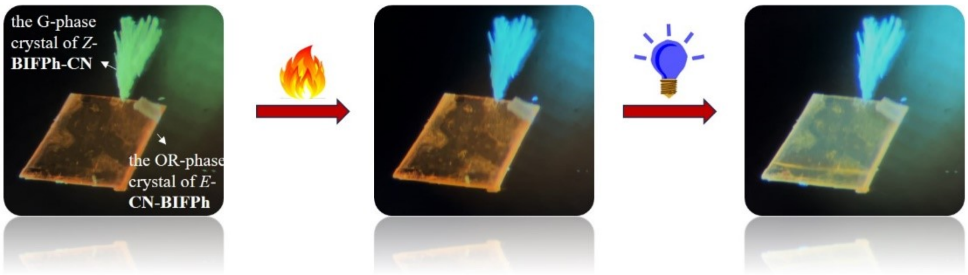

Figure S22 The fluorescence changes of the G-phase crystal of *Z*-**BIFPh-CN** and the OR-phase crystal of *E*-**CN-BIFPh** upon heating and irradiating with 365 nm light.

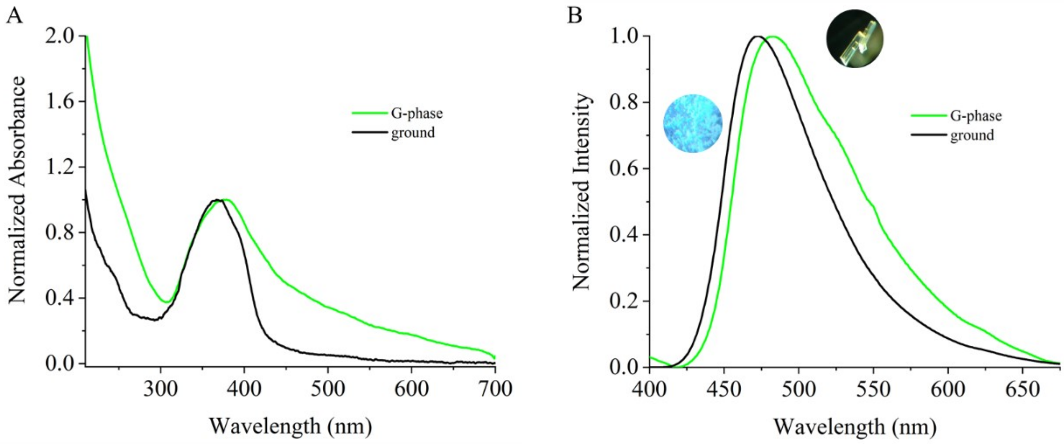

Figure S23 Normalized UV-vis absorbance (A) and fluorescence emission spectra (B, λ_{ex} = 365 nm) of *Z*-**BIFPh-CN** in G-phase crystals before and after being ground. Insets: Optical microscope photos of G-phase crystals of *Z*-**BIFPh-CN** before and after being ground under UV light.

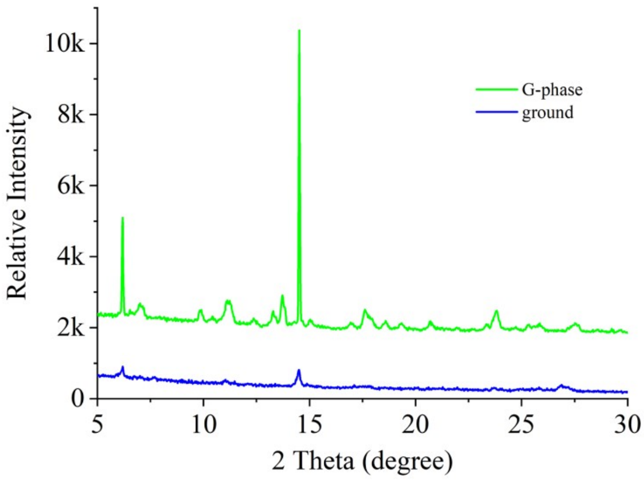

Figure S24 The PXRD pattern of G-phase crystals of *Z*-**BIFPh**-**CN** before (green) and after (blue) being ground.

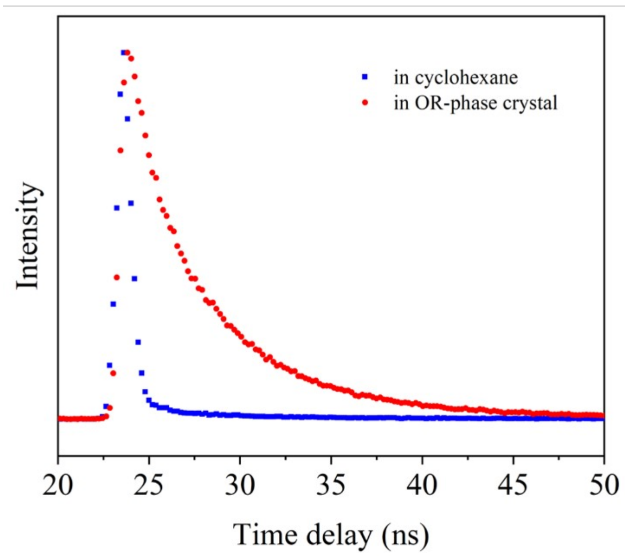

Figure S25 Fluorescence decay curves of *E*-**CN-BIFPh** in cyclohexane and OR-phase crystal.

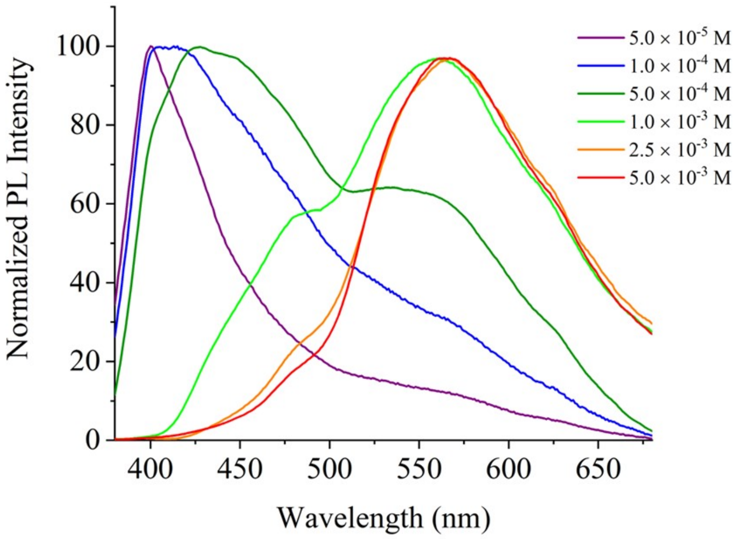

Figure S26 The concentration-dependent emission spectra of *E*-**CN-BIFPh** in THF.

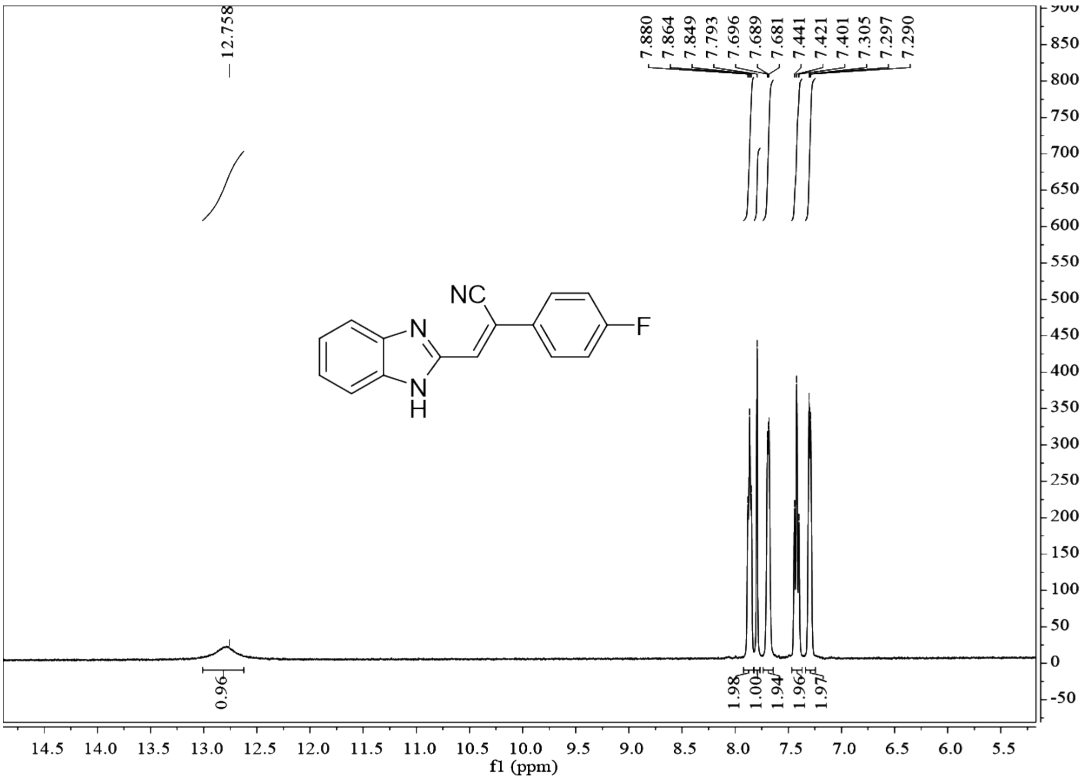

Figure S27 ^{1}H NMR (400 MHz) spectrum of *Z*-**BIFPh-CN** in DMSO-d_6.

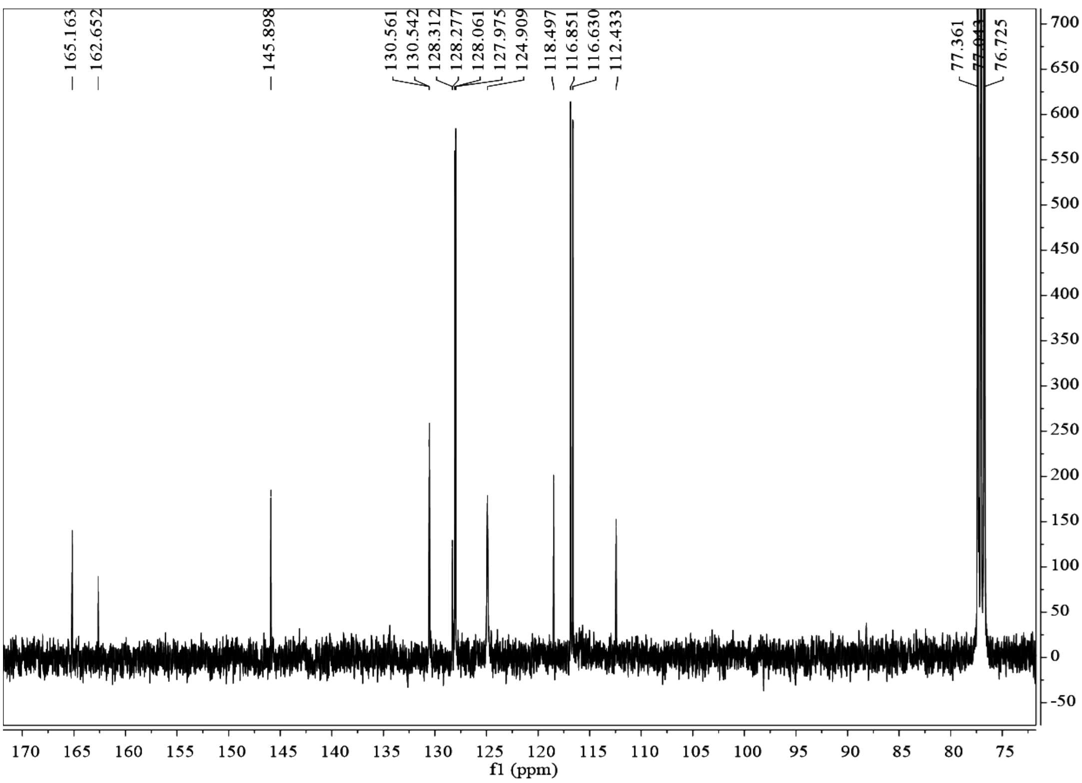

Figure S28 ^{13}C NMR (101 MHz) spectrum of *Z*-**BIFPh-CN** in $CDCl_3$.

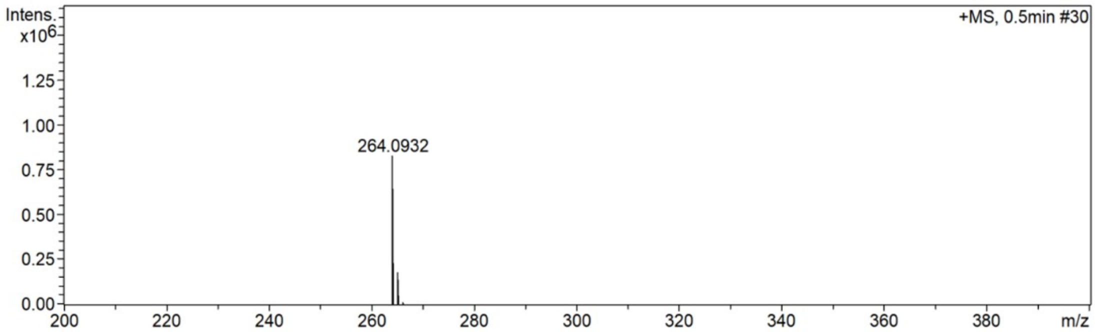

Meas. m/z	#	Formula	m/z	err [ppm]	Mean err [ppm]	rdb	N-Rule	e⁻ Conf	mSigma	Std I	Std Mean m/z	Std I VarNorm	Std m/z Diff	Std Comb Dev
264.0932	1	C 16 H 11 F N 3	264.0932	-0.2	0.4	12.5	ok	even	20.65	0.0353	0.0003	0.0140	0.0007	0.8427

Figure S29 The HRMS of *Z*-**BIFPh-CN**.

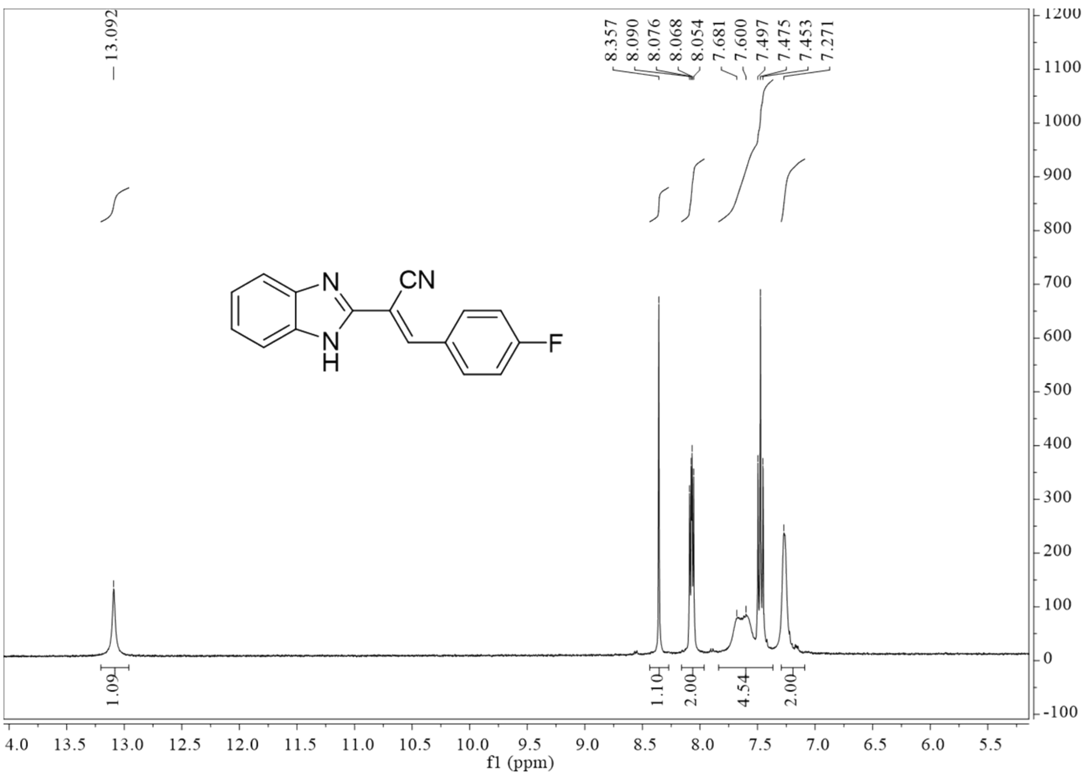

Figure S30 ^{1}H NMR (400 MHz) spectrum of *E*-**CN-BIFPh** in DMSO-d_6.

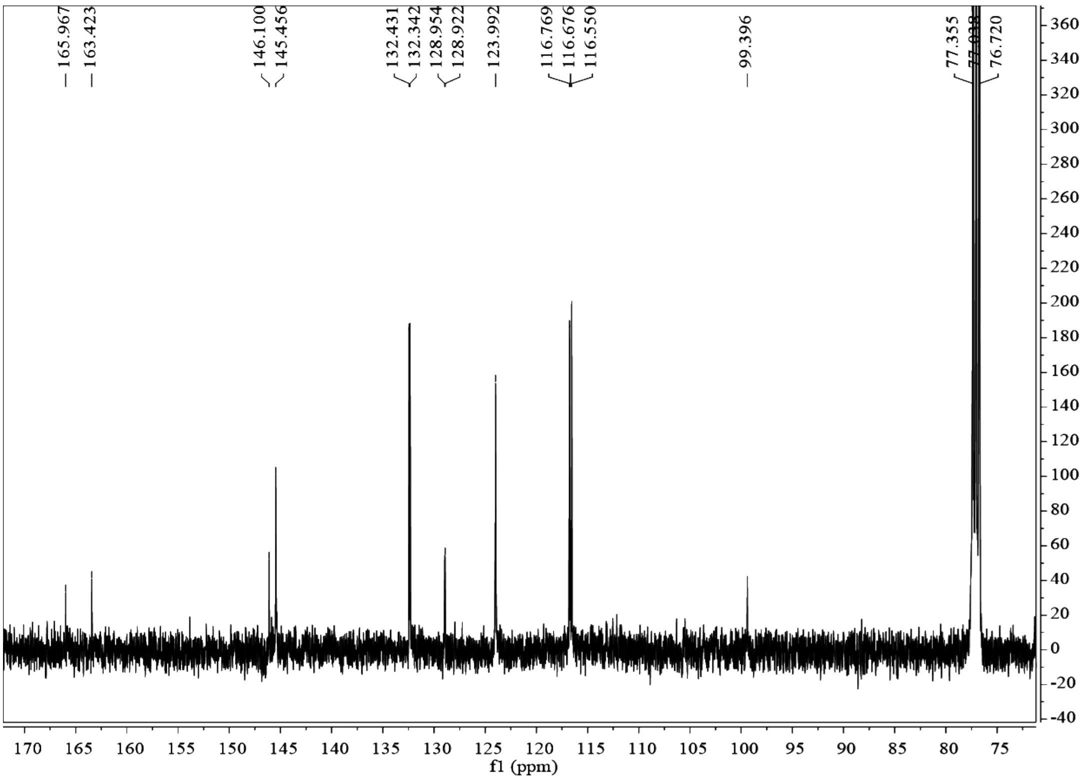

Figure S31 ^{13}C NMR (101 MHz) spectrum of *E*-**CN-BIFPh** in $CDCl_3$.

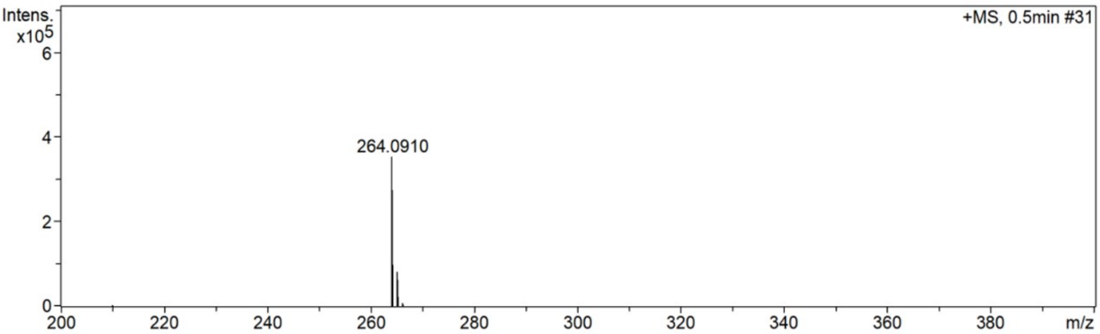

Meas. m/z	#	Formula	m/z	err [ppm]	Mean err [ppm]	rdb	N-Rule	e⁻ Conf	mSigma	Std I	Std Mean m/z	Std I VarNorm	Std m/z Diff	Std Comb Dev
264.0910	1	C 16 H 11 F N 3	264.0932	8.1	9.3	12.5	ok	even	25.89	0.0447	0.0025	0.0176	0.0016	0.8427

Figure S32 The HRMS of *E*-**CN-BIFPh**.

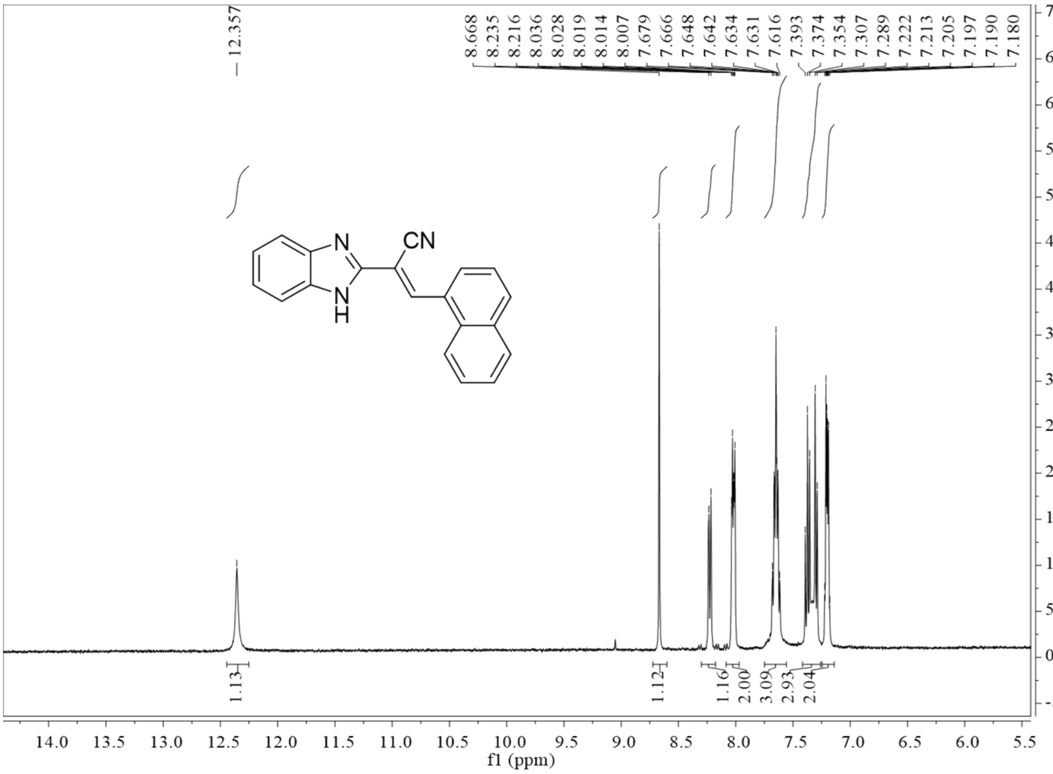

Figure S33 ^{1}H NMR (400 MHz) spectrum of *E*-**CN-BINa** in DMSO-d_6.

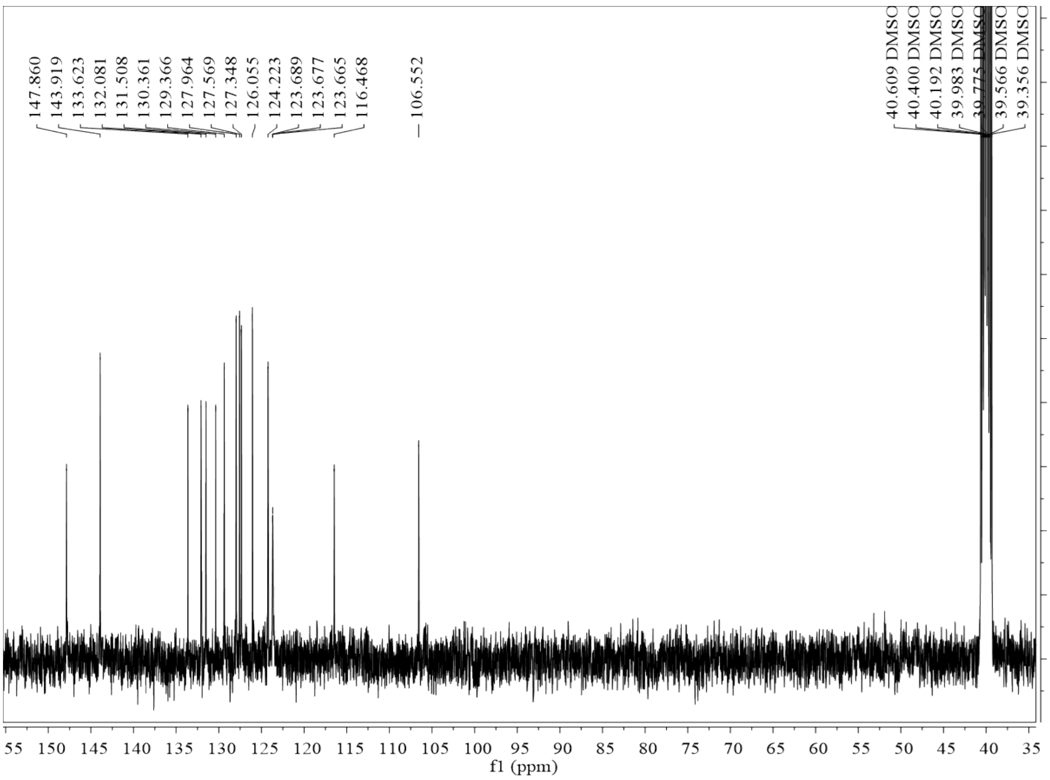

Figure S34 ^{13}C NMR (101 MHz) spectrum of *E*-**CN-BINa** in DMSO-d_6.

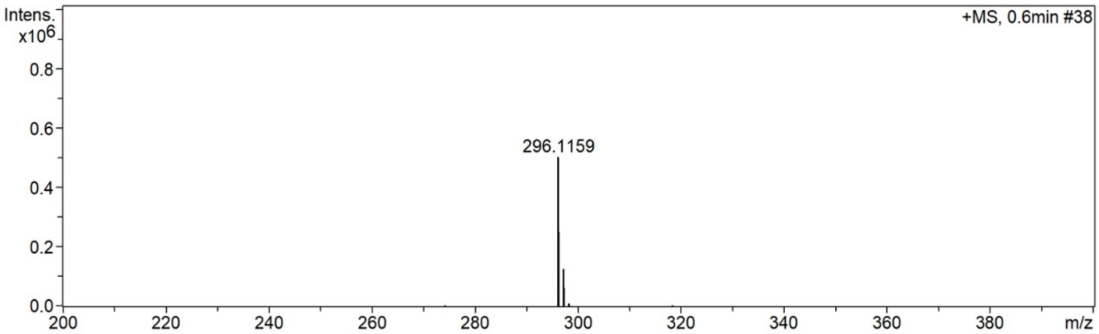

Meas. m/z	#	Formula	m/z	err [ppm]	Mean err [ppm]	rdb	N-Rule	e⁻ Conf	mSigma	Std I	Std Mean m/z	Std I VarNorm	Std m/z Diff	Std Comb Dev
296.1159														
	1	C 20 H 14 N 3	296.1182	8.0	8.9	15.5	ok	even	12.66	0.0195	0.0027	0.0080	0.0011	0.8427

Figure S35 The HRMS of *E*-**CN-BINa**.

References

[1] R. Dennington, T. A. Keith, J. M. Millam, GaussView, Version 6, Semichem Inc., 2016.

[2] M. J. Frisch, G. W. Trucks, H. B. Schlegel, G. E. Scuseria, M. A. Robb, J. R. Cheeseman, G. Scalmani, V. Barone, G. A. Petersson, H. Nakatsuji, X. Li, M. Caricato, A. V. Marenich, J. Bloino, B. G. Janesko, R. Gomperts, B. Mennucci, H. P. Hratchian, J. V. Ortiz, A. F. Izmaylov, J. L. Sonnenberg, Williams, F. Ding, F. Lipparini, F. Egidi, J. Goings, B. Peng, A. Petrone, T. Henderson, D. Ranasinghe, V. G. Zakrzewski, J. Gao, N. Rega, G. Zheng, W. Liang, M. Hada, M. Ehara, K. Toyota, R. Fukuda, J. Hasegawa, M. Ishida, T. Nakajima, Y. Honda, O. Kitao, H. Nakai, T. Vreven, K. Throssell, J. A. Montgomery Jr., J. E. Peralta, F. Ogliaro, M. J. Bearpark, J. J. Heyd, E. N. Brothers, K. N. Kudin, V. N. Staroverov, T. A. Keith, R. Kobayashi, J. Normand, K. Raghavachari, A. P. Rendell, J. C. Burant, S. S. Iyengar, J. Tomasi, M. Cossi, J. M. Millam, M. Klene, C. Adamo, R. Cammi, J. W. Ochterski, R. L. Martin, K. Morokuma, O. Farkas, J. B. Foresman, D. J. Fox, Gaussian 16 Rev. C.01, Wallingford, CT, 2016.

[3] T. Lu, F. Chen, *J. Comput. Chem.* **2012**, *33*, 580-592.